Arabian Journal of Geosciences (2021) 14:554
https://doi.org/10.1007/s12517-021-06918-6

ORIGINAL PAPER

The differential evolution of nanopores in discrete OM and organic-clay composites for shale: insights from stress manipulation

Yuantao Gu[1] · Xiaoxia Li[1] · Quan Wan[2] · Shuguang Yang[2,3]

Received: 5 October 2020 / Accepted: 9 March 2021

Abstract

The organic carbon in shale has been proved to be a significant hydrocarbon source in two occurrences of discrete OM and organic-clay composites. Although the evolution of OM-hosted pores has been investigated by extensive research, the evolution of nanopores in discrete OM and organic-clay composites under additional stress is still unclear. In this study, two potential shales in China (Silurian Longmaxi (S_1l) formation and Cambrian Niutitang ($Є_1n$) formation) were selected to examine the nanopores characteristics developed in discrete OM and organic-clay composites using field emission scanning electron microscopy (FE-SEM) and statistical analyses. The microstructure observations of the two shales show that during the growth of nanopores, the expansion of nanopores in composites was restricted by the narrow space between clay layers, and then, the nanopores would be protected from collapse or compaction by clay layers with further maturity. The discrete OM particles constantly suffer squeezing from brittle minerals and lead to the nanopores thrown into compressive environment, resulting in a preferred orientation along the edge of mineral particles and narrowing shape, as well as diminishing the pore sizes. For organic-clay composites, the development of nanopores is determined by additional stress state. Under compressive stress, no pores could be observed, while the nanopores are widely distributed in tensile environment or stress-free state. Consequently, the nanopores development in discrete OM and organic-clay composites are significantly affected by additional stress. The research findings imply the potential hydrocarbon source in the nanopores located in organic-clay composites and would bring inspiration for the exploitation of shale gas.

Keywords Shale · Nanopores · Discrete OM · Organic-clay composites · Evolution · Stress

Introduction

Organic matter (OM) has been proved to affect ultimately a shale's ability to generate, store, and produce hydrocarbons since the discovery of nanopores in OM using ion milling and FE-SEM (Loucks et al. 2009), indicating OM was considered a contributor to the porosity network. As previously studied, two occurrences are found for organic carbon in shale: discrete OM and organic-clay composites. Most of discrete OM are relatively independent of minerals in the form of kerogen, while organic-clay composites are the products of the complexation of organic carbon and clay minerals.

Organic-clay composites, as a significant hydrocarbon source, account for the primary fraction of the sedimentary OM in source rocks (Cai et al. 2013; Lu et al. 2013; Kennedy et al. 2014; Rahman et al. 2018; Zhu et al. 2018). The mineral surface control of organic carbon in black shales suggests that the dominant association of organic carbon is with mineral surfaces and not as discrete pelagic grains by the strong positive relation between total organic carbon (TOC) and mineral surface area (MSA) over a range of 15% TOC (Kennedy et al. 2002, 2014). The interlayer sites of clay minerals are also accessible to polar and non-polar organics, ions, and water because of the expandable clay interlayer (Theng et al. 1986; Sposito et al. 1999; Jia et al. 2002; Chen

Responsible Editor: Santanu Banerjee

✉ Yuantao Gu
guyuantao@haue.edu.cn

[1] School of resource and environment, Henan University of Engineering, Xianghe Road 1, Zhengzhou 451191, Henan, China

[2] State Key Laboratory of Ore Deposit Geochemistry, Institute of Geochemistry, Chinese Academy of Sciences, Guiyang 550081, Guizhou, China

[3] University of Chinese Academy of Sciences, Beijing 100049, China

Published online: 19 March 2021

et al. 2008). The incorporation of molecular-scale organic compounds (derived from the physical or chemical break down of organic particles) in the clay interlayer space has thus been hypothesized to protect organic carbon from microbial degradation (Kennedy et al. 2002; Kennedy and Wagner 2011). Significant information from classifying stable and mobile of organic matter in organic-clay composites have been achieved to indicate that stable organic carbon mainly occurs on the mineral internal surface and mobile organic carbon mainly adsorbed on the mineral external surface (Zhu et al. 2016, 2018). The above researches verified organic-clay composites are the important carriers for OM and play a significant role in preserving organic carbon. In addition, organic-clay composites have an important effect on promoting the exploitation of hydrocarbons. For example, the combination of OM and clay minerals seriously affected the pyrolysis reaction of OM, and further made a difference in the yield and composition of hydrocarbons (Bu et al. 2017). Furthermore, during the maturation of organic-clay composites, a significant amount of free silica could be generated from the smectite illitization, which may well prove to be a critical factor for formation fracking efficiency (Berthonneau et al. 2016).

Above all, organic-clay composites play an important role in the generation and development of shale gas. However, the impacts of organic-clay composites on the storage of hydrocarbons have still not been investigated, which maybe make a big difference for the gas in place. As well known, OM nanopores, as the main reservoir space, have decisive influence on the generation, storage, and seepage of shale gas (Loucks et al. 2009; Nelson 2009; Chalmers et al. 2012; Curtis et al. 2012b). It is worth noting that previous studies have found nanopores are well developed in organic-clay composites and mostly are OM pores (Gu et al. 2017, 2018), which imply the attributes of organic-clay composites in generation and occurrence of hydrocarbon. Significantly, nanopores in discrete OM could be deformed under additional stress. For example, OM particles under compressive forces could diminish the sizes of pores and flatten them from spherical to ellipsoidal along a preferred orientation (Wang 2020). However, the effects of additional stress on organic-clay composites and its internal nanopores are still unclear.

To answer the above questions, in present study, we investigated the differences of nanopores characteristics between discrete OM and organic-clay composites under additional stress. Two series of mud rocks from economically valuable strata in China (Silurian Longmaxi (S_1l) formation, and Cambrian Niutitang ($Є_1n$) formation) were collected, which have been demonstrated the great potential of shale gas (Guo et al. 2014; Tang et al. 2015; Dong et al. 2016; Wang et al. 2016). Through elaborate observation of field emission scanning electron microscopy (FE-SEM) and statistical analyses, we specify the differences of nanopores characteristics between organic-clay composites and discrete OM, and then explore the developing characters of nanopores under various stresses. As will be shown, the results would bring significant implications for reservoir evaluation and exploitation of shale gas.

Samples and methods

Samples

A total of twenty-eight samples from S_1l and $Є_1n$ formations were collected to carry out this research. Figure 1 shows the locations of the two sampling sites and region geology. Fourteen samples of S_1l shales were mined at a half meter to one-meter-deep to insure the freshness of samples by a Shaw Core Sampling Backpack Drill in Xishui, Guizhou Province, located in the eastern of Dian-Qian North Depression (sampling site (A) in Fig. 1). S_1l shales in here are segmented into three members and the first member is the main production layer for shale gas. Therefore, all the S_1l shales are collected from the first member, which is divided into eight layers (from 2th layer to 9^{th} layer, and the first layer is located in Wufeng Formation (O_3w) of Ordovician). According to the vertical thickness of each layer, as shown in Table 1, fourteen shallow drills (i.e., fourteen samples) are distributed evenly over the eight layers. The $Є_1n$ shales samples were obtained from a drill in Kaiyang, Guizhou Province, located in the east of Central Guizhou Uplift (sampling site (B) in Fig. 1), which is surrounded by Dian-Qian North Depression, Wuling Depression, South Guizhou Depression, and Southwest Guizhou Depression. The stratigraphic characteristics and the corresponding sampling locations are shown in Fig. 2.

TOC

The TOC of the samples were measured by using a vario MACRO cube organic element analyzer following the Chinese Oil and Gas Industry Standard GB/T19145-2003. The samples are crushed and ground to 200 mesh. Then, the inorganic carbon in the powders was eliminated before the measurement by over adding diluted hydrochloric acid at a ratio of HCl: H_2O = 1:7 (V/V). The measurements were performed at the Analysis and Testing Center, Henan University of Engineering.

Thermal maturity

Laser Raman spectroscopy has been evidenced as a suitable method to calculate the reflectance by previous researches on thermal maturity (Kelemen and Fang 2001; Tuschel 2013; Chen et al. 2015). A Renishaw Invia Reflex Laser Raman Spectrometer at Analysis and Testing Center, Henan University of Engineering, was used to measure the reflectance values of the polished samples. In this work, the

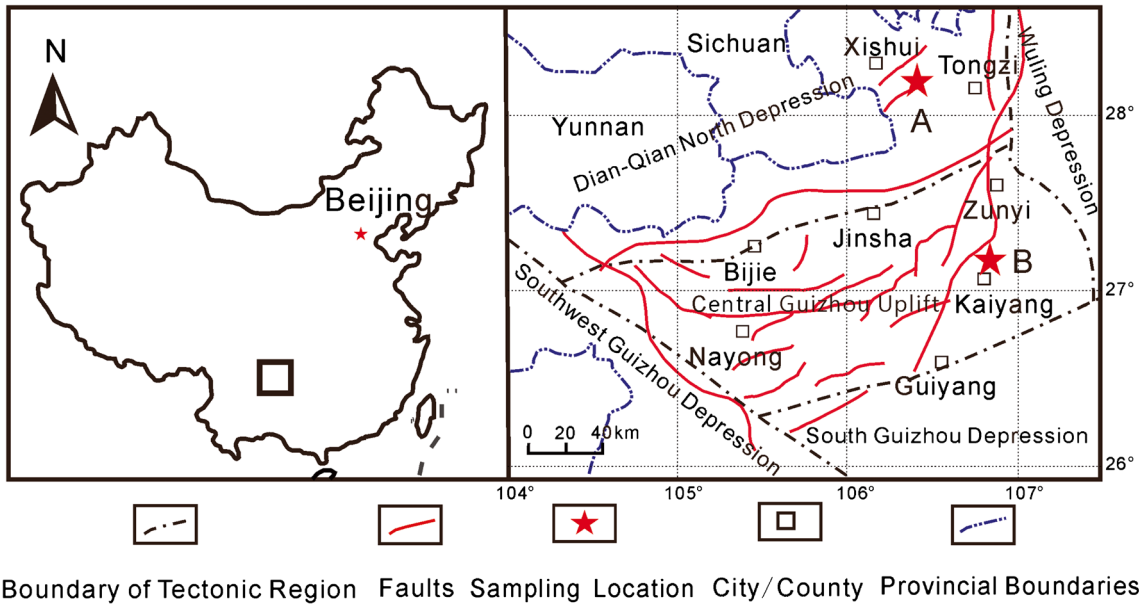

Fig. 1 The locations of the sampling sites and regional geology (Modified from Lu et al. 2015)

calculation of reflectance values (R) follows the equation:

$$R = 0.0537\, d\,(G{-}D){-}11.21, \quad (1)$$

where G, D, and $d(G\text{-}D)$ denote peak positions of the graphitic carbon and disordered carbon and the interpeak intervals between G and D, respectively (Kelemen and Fang 2001; Liu et al. 2012). Due to the absence of vitrinite in the Lower Paleozoic marine shales, for S_1l and ϵ_1n shales, the bitumen reflectance (R_b) was measured to identify the thermal maturity of samples. According to the relationship between R_b and R_o, the relation

$$R_o = (R_b + 0.2443)/1.0495, \quad (2)$$

is used to calculate R_o (Schoenherr et al. 2007).

Mineralogical composition

A Bruker D8 ADVANCE X-ray diffractometer (XRD) in the Analysis and Testing Center, Henan University of Engineering, was used to determine the mineralogical composition of the powder samples. The testing angle ranged from 5° to 90°. The results were analyzed quantitatively following the Chinese Oil and Gas Industry Standard (SY/T) 5163-2010.

FE-SEM

Before the SEM observation, the samples were polished by a Leica EM TIC 3X argon-ion polisher to obtain a smooth surface. Then, the samples were sputter-coated with gold. An FEI Scios FE-SEM at Center for Lunar and Planetary Sciences, Institute of Geochemistry, Chinese Academy of Sciences, operated at an acceleration voltage of 20 kV, was used to characterize the microstructure of the shale samples.

Results

Sample composition

The sampling locations, burial depth, R_o, and TOC of the samples are shown in Table 1. For S_1l shales, except for the 6th and 7th layers collected only one sample, the other layers are selected two sampling locations in upper and lower of the layer. The ϵ_1n shales are collected every few meters from up to bottom in the range of sixty meters. TOC contents of the two groups of samples range from 0.37 to 5.48% for S_1l shales and from 0.33 to 5.52% for ϵ_1n shales with average values of 2.97% and 2.51%, respectively, indicating most of the samples are organic-rich shale (>2.0%). Besides, a commonality occurred between S_1l and ϵ_1n shales is that TOC contents present a remarkable increase trend from the top-down, signifying the water depth of sedimentation varies from shallow to deep and probably implying the better hydrocarbon potential of lower strata. The R_o values vary from 2.56 to 2.91% for S_1l shales and from 2.86 to 3.32% for ϵ_1n shales with 2.79% and 3.06% on average, respectively, suggesting that the two formations are in high or over maturation.

The mineralogical compositions of the selected shale samples are also listed in Table 1. The two groups of shales consist mainly of quartz, clay minerals (including illte, I/S, kaolinite, and chlorite), and feldspar, as well as a small amount of pyrite and carbonate. The ternary diagram (Fig. 3) illustrates a comparison of the mineralogical constituents (quartz and feldspar,

Table 1 The sampling location, burial depth, TOC, R_o, and mineralogical composition of the samples

Sample ID	Sampling location/burial depth	TOC (%)	R_o (%)	Mineralogical composition					
				Quartz (%)	Clay (%)	Feldspar (%)	Pyrite (%)	Calcite (%)	Dolomite (%)
L-1	upper of 9th layer/0.6	0.63	2.79	31.6	44.3	14.1	<1.0	8.5	nd
L-2	lower of 9th layer/0.6	0.61	2.86	34.0	45.4	12.9	<1.0	5.2	1.6
L-3	upper of 8th layer/0.6	0.37	2.82	35.8	50.4	10.3	<1.0	1.5	1.2
L-4	lower of 8th layer/0.6	1.04	2.89	35.1	32.9	27.5	<1.0	2.6	1.1
L-5	7th layer/0.6	1.75	2.85	36.7	28.9	26.9	1.2	4.6	1.7
L-6	6th layer/1.0	1.94	2.91	37.9	32.8	20.4	1.9	5.4	1.5
L-7	upper of 5th layer/0.5	3.00	2.85	57.9	18.2	14.5	2.7	5.3	1.5
L-8	lower of 5th layer/0.6	3.01	2.56	45.5	26.4	16.4	3.4	5.9	2.4
L-9	upper of 4th layer/0.6	2.73	2.88	52.4	19.7	16.5	2.1	5.9	3.3
L-10	lower of 4th layer/0.4	3.29	2.63	54.7	20.3	15.7	2.2	5.1	1.9
L-11	upper of 3th layer/0.5	3.69	2.74	76.3	10.6	13.1	nd	nd	nd
L-12	lower of 3th layer/0.4	4.58	2.75	67.6	16.9	12.5	2.0	nd	<1.0
L-13	upper of 2th layer/1.0	5.48	2.86	55.9	16.7	17.6	1.9	4.4	3.4
L-14	lower of 2th layer/0.5	4.75	2.64	42.7	21.3	22.0	2.2	3.8	8.1
N-1	656.8	0.39	2.98	39.8	43.6	15.1	1.5	nd	nd
N-2	658.5	0.39	3.11	43	39.7	15.5	1.8	nd	nd
N-3	662.0	0.71	2.96	42.8	42.0	13.7	1.6	nd	nd
N-4	668.4	1.27	3.12	48.8	34.4	13.1	1.6	1.4	<1.0
N-5	670.0	1.38	3.32	45.6	36.1	14.6	1.6	1.2	<1.0
N-6	672.4	1.23	3.22	45.5	36.8	14.8	1.3	<1.0	<1.0
N-7	699.6	0.33	3.10	41.2	38.2	14.5	1.8	3.4	nd
N-8	683.1	0.35	2.93	43.4	38.6	14.1	1.7	1.6	<1.0
N-9	691.7	3.42	3.01	49.9	32.2	7.9	2.1	2.0	2.9
N-10	694.1	2.43	3.13	45.0	31.5	14.2	2.3	2.3	4.9
N-11	698.4	5.52	2.86	42.0	23.7	28.5	3.9	nd	1.9
N-12	701.0	4.22	3.0	36.6	19.9	31.7	2.7	nd	9.1
N-13	708.6	4.94	3.04	42.8	35.7	10.5	7.9	nd	3.2
N-14	717.8	4.24	3.0	46.5	35.3	7.3	6.3	nd	4.5

"*nd*" noted not detected

clay, carbonate) of the two groups of shales examined in this study. Generally, as shown in Fig. 3, the S_1l shales have higher contents of quartz and feldspar (averaging 64.6%), and carbonates (averaging 6.1%) than $Є_1n$ (averaging 59.5% of quartz and feldspar, and averaging 2.7% of carbonates), while contrast with $Є_1n$ shales (averaging 34.8%), lower contents of clay minerals can be found in S_1l shales (averaging 27.5%).

Microstructure characteristics of organic-clay composites

The microstructure characteristics of the two groups of samples can be seen in Fig. 4 and Fig. 5. Both the two formations present multitudinous attributes of potential shale. For example, the distribution of OM, clay minerals, and brittle minerals particles demonstrate the strong heterogeneity in material composition. As mentioned earlier, discrete OM and organic-clay composites are the two main occurrences for organic carbon. The discrete OM particles in the observed samples mostly fill between skeleton particles strengthens the compression resistance of the debris mineral grains and present irregular shapes. Of particular note is the widespread organic-clay composite, exhibiting various morphologies. According to whether composites are deformed or not, the composites could be classified into two types: primary and deformed. The primary composites note the original forms which have not suffer distorting under additional force after diagenesis, mainly including band-like and "cardhouse." The band-like composites (Fig. 4a and d, Fig. 5f) are of obvious bed-parallel extension. Their formation presumably starts from that clay minerals sediment in the manner of face/face

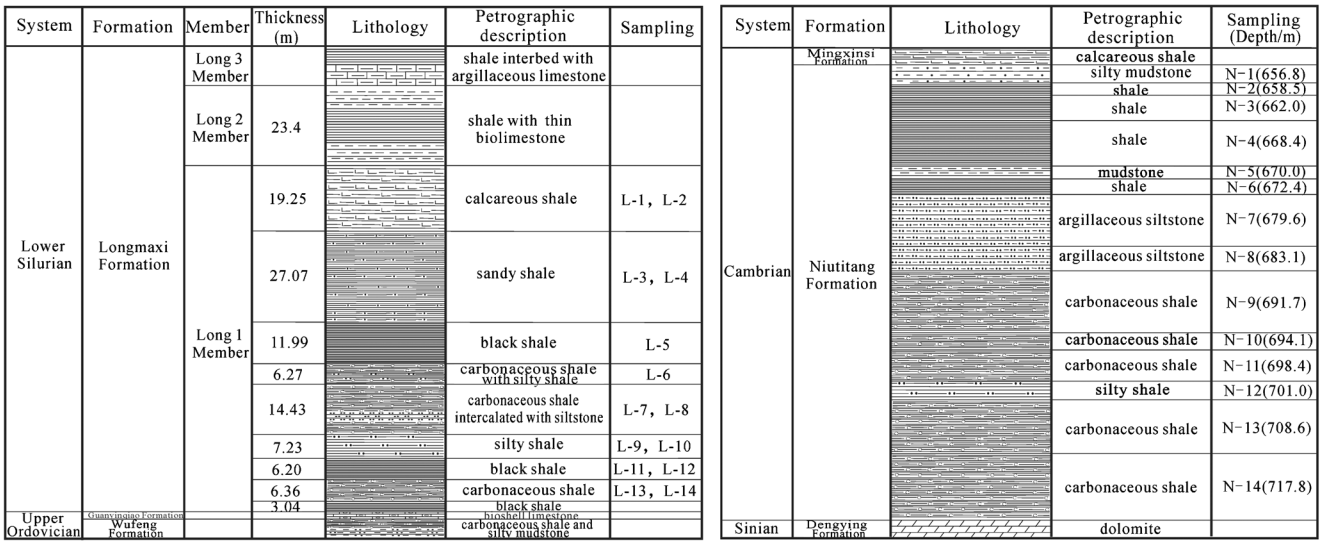

Fig. 2 The stratigraphic characteristics and the corresponding sampling locations (the left denotes Longmaxi Formation, and the right denotes Niutitang Formation)

contacts (band-like structures) in an alkaline medium (O'Brien 1971; Lagely 1989), and then, organic carbon intercalates the interlayer space of clay minerals during diagenesis and thermal evolution under certain strata pressure (Kennedy et al. 2014). The "cardhouse" composites are also a common form in S_1l and ϵ_1n shales (Fig. 4c, Fig. 5b), which have a different forming environment with band-like composites. In an acidic medium, due to the differential charge of clay minerals, the end face adsorbed on the surface of clay layers, and then formed edge/face contacts, i.e., the "cardhouse" structure, which has been interpreted as a primary depositional feature, and their preservation could be ascribed to passive pore filling (probably biological fossils) prior to the significant compaction of clays (O'Brien 1971; Lagely 1989; Day-Stirrat et al. 2008; Liu et al. 2019). After the formation of primary composites, under the effect of stress, probably derived from tectonic movement, mineral transformation, and thermal maturation of OM, most composites appear deformed to various shapes, such as triangle (Fig. 4g), lenticular (Fig. 4b, Fig. 5h), as well as irregular (Fig. 4h and i, Fig. 5g–i). As presented by Fig. 4b and g, as well as Fig. 5g and h, the plasticity of clay layers decides that most deformations of composites are plastic rather than brittle.

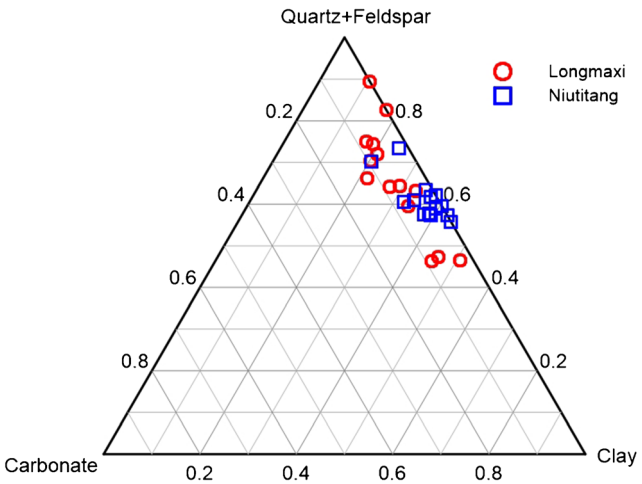

Fig. 3 Ternary diagram showing a comparison of the mineralogical constituents of the two shales examined in this study

Another interesting commonality for the two shales is the distribution of pyrites in organic-clay composites (Fig. 4a, b, d, g, and Fig. 5e, g, h). We suggest that the pyrites emerge during the thermal evolution of composites. Some organic molecules, in the form of organic sulfur compounds, were preferentially associated with the smectite layers (Berthonneau et al. 2016). As sediments are buried, Fe^{3}+ in Al–O octahedron of clay mineral tends to be reduced progressively to the ferrous state through the decarboxylation in the process of OM degradation (Devey and Curtis 1989), which promote Fe^{2+} bond with sulfur originated in organicsulfur compounds during thermal evolution. Consequently, most of pyrites are generated parallel to the clay layers as short rod-like particles and stuck between the clay layers rather than distribute the outside of composites.

Development characteristics of nanopores in discrete OM and organic-clay composites

The nanopores in various carriers present quite different development characteristics in the two formations. In this study, pores in discrete OM and organic-clay composites are the main objects for comparison. At first, the two groups of samples have obvious difference in the development of nanopores in discrete OM. Figure 4c, e, f, h, and i demonstrates the prevalence of various shapes of OM pores in S_1l shales. Quite different with S_1l shales, ϵ_1n shales show large amounts of non-porous OM (Fig. 5a, c, d), which is caused by the

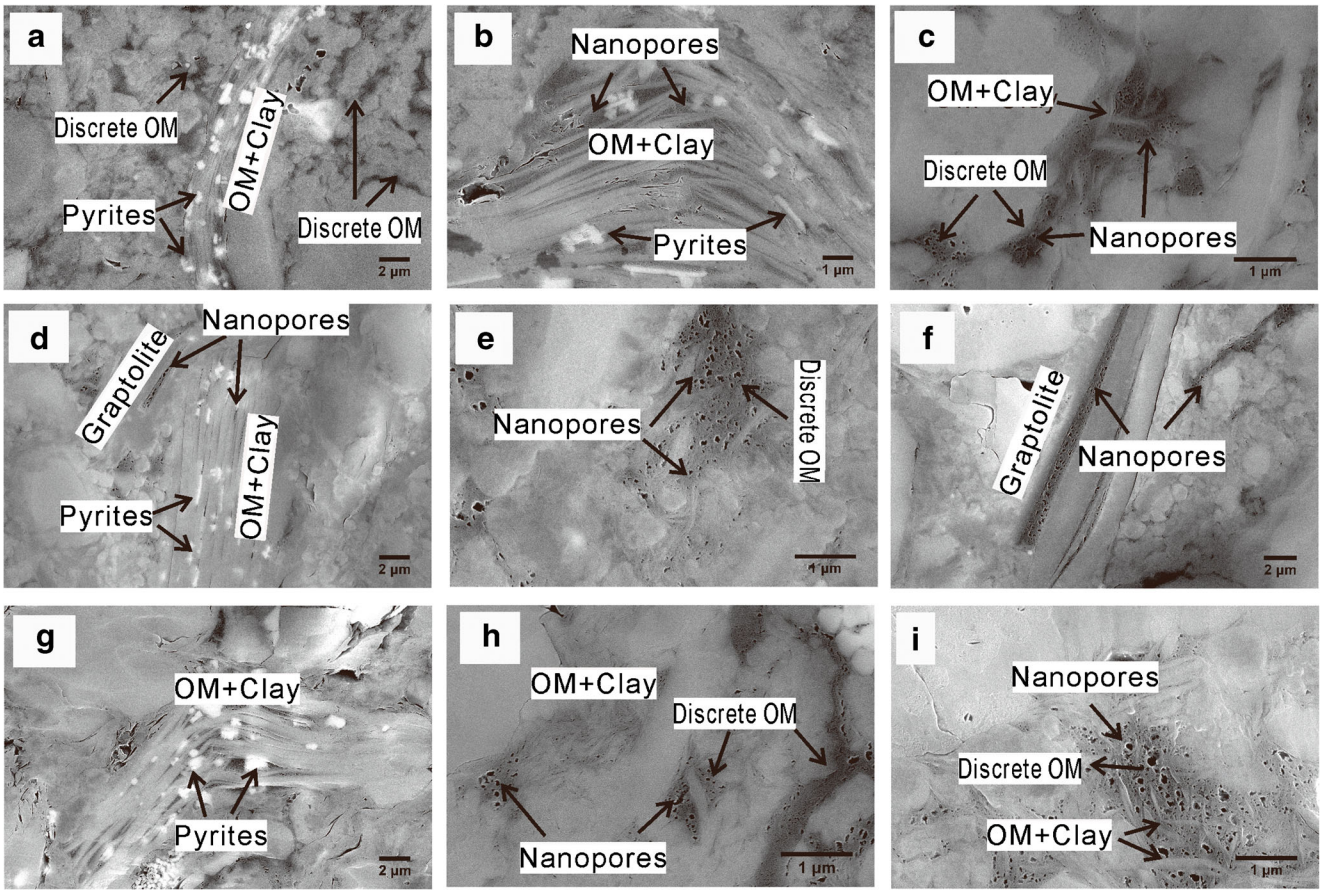

Fig. 4 The FE-SEM images of microstructure for S_1l shales

complete gas expulsion (pore collapse) as a consequence of greater OM connectivity and framework compaction, and ulteriorly attributed to the over-maturation and the greater strata pressure from palaeoburial depths (6500 m for S_1l and 9000 m for $Є_1n$) (Curtis et al. 2012a; Milliken et al. 2013; Chen and Xiao 2014; Liu et al. 2016; Wang et al. 2016). Secondly, nanopores in organic-clay composites behave different features with discrete OM. Numerous nanopores developed in composites for both S_1l and $Є_1n$ shales. Take account of quantities of non-porous OM particles in $Є_1n$ shales (Fig. 5a, c, d), we supposed that organic-clay composites protect the nanopores from collapse and compaction in the condition of higher maturity and deeper palaeoburial depths compared to S_1l shales.

The above information indicates that with increasing thermal maturity, nanopores in organic-clay composites perform different evolutionary trends with discrete OM. To quantitative study the pore size, statistical analyses according to the gray difference by the Image J software were performed to analyze the pore characteristics in the range of 5–500 nm within a certain region. As Fig. 6 illustrates, four regions in the two FE-SEM images are selected to ascertain the difference of pore size between discrete OM and composites in S_1l shales. The four grayscale maps (Fig. 6 A_1, A_2, B_1, B_2) present the distribution characteristics of pores, and the quantitative results are listed in Table 2, which demonstrates a universal regularity that the nanopores in discrete OM (Fig. 6 A_1 and B_1 (diameters of 29 nm and 30 nm, respectively)) are larger than that in composites (Fig. 6 A_2 and B_2 (diameters of 21 nm and 23 nm, respectively)). The differences of pore size between discrete OM and composites suggest that composites restrict the development of nanopores. During the growth of nanopores, the clay layers are likely to hinder the expansion of nanopores because the tiny OM particles between clay layers are adverse to the pore growth (Milliken et al. 2013).

Nevertheless, different situations occur in $Є_1n$ shales. Although little nanopores could be found in discrete OM (Fig. 5a, c, d), under the over-compaction of strata and over maturation of OM, nanopores are still well-developed in composites (Fig. 5b, f, i). To quantitative compare the pore size, as presented in Fig. 7, two regions (Fig. 7c, d) where nanopores developed relatively well in discrete OM, and two porous composites (Fig. 7e, f) are marked for the statistical analyses of pores. Coincidentally, as Table 3 shows, there is not much difference in pore size between discrete OM (Fig. 7 C_1 and D_1 (diameters of 18 nm)) and composites (Fig. 7 E_1 and F_1 (diameters of 18 nm and 17 nm, respectively)). Contrast with S_1l shales, the average pore diameters in discrete OM present a

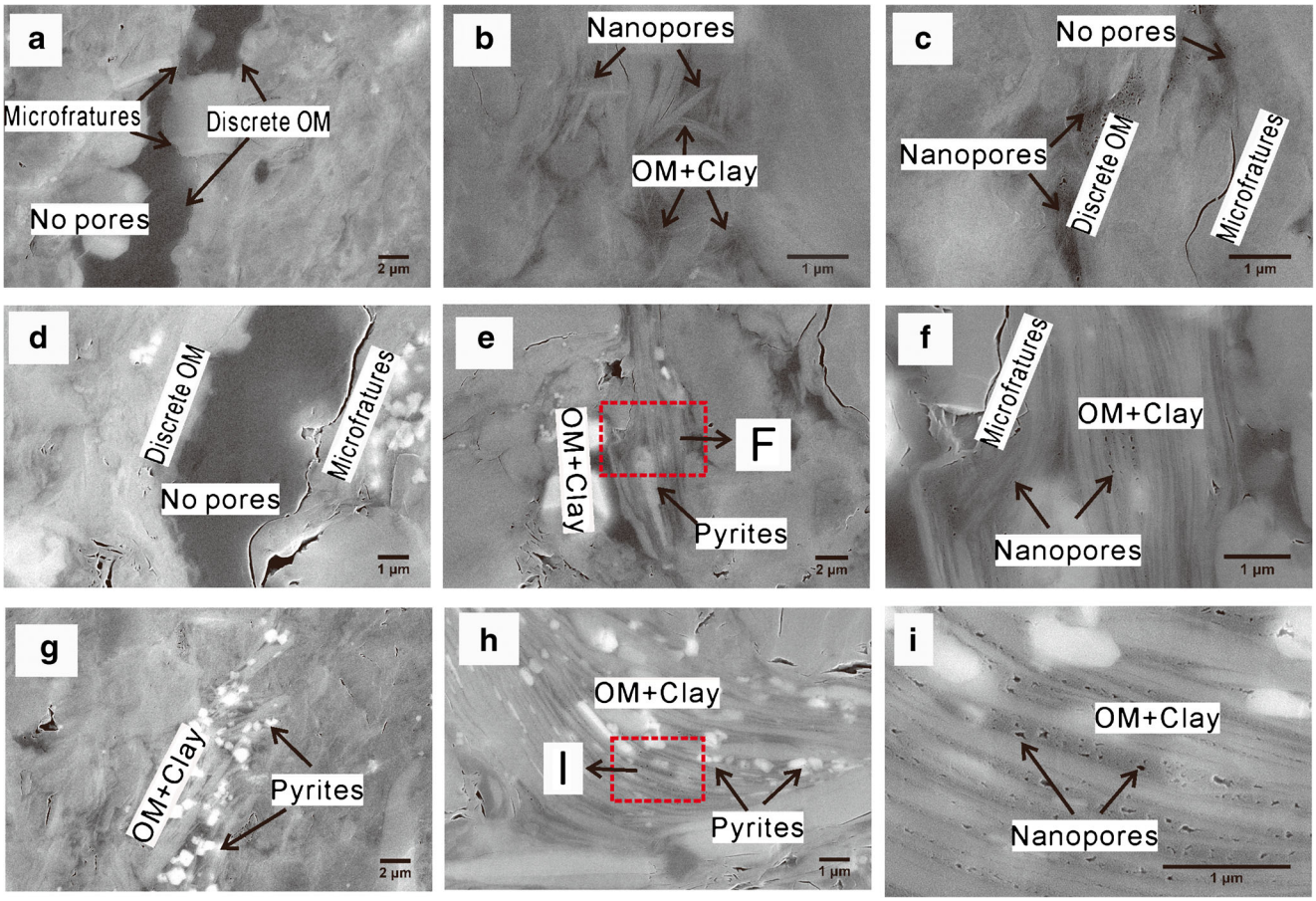

Fig. 5 The FE-SEM images of microstructure for ϵ_1n shales

dramatic decrease for ϵ_1n shales. Coupled with the dominant non-porous discrete OM in ϵ_1n shales, the decrease tend of pore size in discrete OM should also be attributed to relative complete gas expulsion and framework compaction (Milliken et al. 2013; Wang et al. 2016). Unlike the pores in discrete OM, the average pore diameters in composites between ϵ_1n and S_1l shales are sufficiently close to each other. Above evidences confirm that clay layers could protect the nanopores in composites from collapse or compaction in over-maturation stage. Three attributes of clay minerals in composites lead to the protection on nanopores. The first one is the high capillary pressure of the narrow space (ranging from several to hundreds of nanometers) between clay layers (Fig. 6 A_2 and B_2, Fig. 7 E_1 and F_1), which is beneficial to form strong adhesion between clay layers and OM (Alcover et al. 2000; Li et al. 2016), and thereby prevent the shrinkage of OM. The second is the structural stability of the inorganic/organic nanohybrids (Chen et al. 2008), which could resist to overburden pressure more robust than discrete OM particles. The last one is the isolation of clay layers on nanopores, leading to the internal pressure in pores could be maintained to prevent the pore spaces from compaction (Milliken et al. 2013).

Table 2 The pore parameter characteristics of statistical regions in Fig. 6

Location	Pore count	Average pore area (nm^2)	Average pore diameter (nm)
A_1	190	424	29
A_2	350	151	21
B_1	167	394	30
B_2	231	182	23

Discussions

The evolution of nanopores in discrete OM and organic-clay composites

Pore connectivity, as a critical factor in shale gas migration and production, can affect gas molecules diffusion, and limit the gas production rate and hydrocarbon recovery (Hu et al. 2012; Guo et al. 2015; Sun et al. 2017). The connectivity of nanopores in shale matrix controls the accessible porosity and matrix diffusion rate (Ruppert et al. 2013; King et al. 2015; Sun et al. 2017). As mentioned earlier, although organic-clay composites have been confirmed the protecting effects on

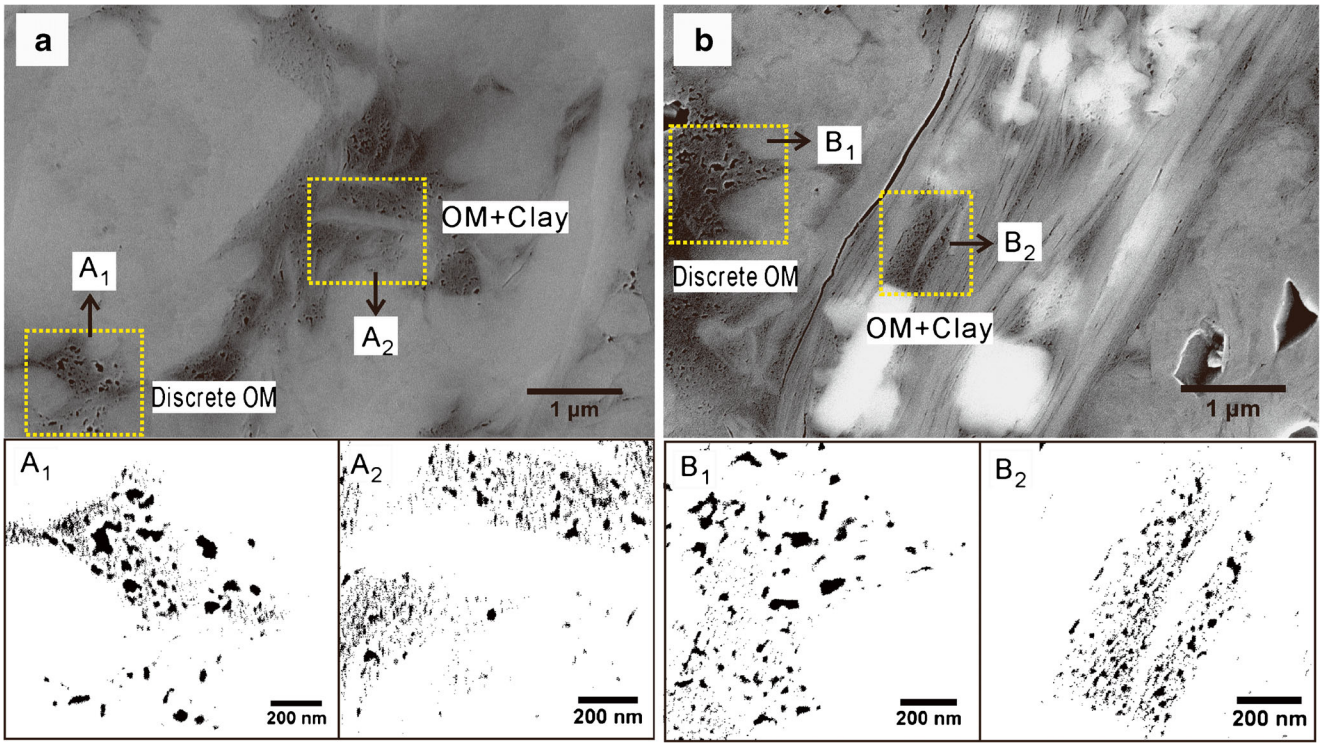

Fig. 6 The nanopores characteristics in discrete OM and organic-clay composites for S_1l shales. The four white dashed rectangles were the selected regions for the statistics of nanopores. A_1–B_2 denoted the grayscale maps of corresponding regions

nanopores, the impacts on pore connectivity have still not been documented. Previous studies have evidenced the high connectivity of OM pores, probably result from the extreme development of pore throats (King et al. 2015; Sun et al. 2017). However, with increasing maturity, the high pore connectivity is conducive to the escape of gas molecules by reason of the development of microfractures between discrete OM and inorganic minerals. Consequently, gas expulsion occurs, meaning the internal pressure in pores decrease and then be inadequate to resist the external geostress. Just like the ϵ_1n shales, no pores housed in discrete OM if microfractures distribute between the OM and adjoining minerals (Fig. 5a, c, d, and Fig. 7a). When no microfractures emerge between OM and minerals, nanopores develop very well in discrete OM (Fig. 7c, d). The reason for the phenomenon is that the OM particles are surrounded closely by adjacent minerals, signifying there is no escape passage for hydrocarbons, so that pores could be supported by internal pressure rather than be compacted (Milliken et al. 2013). For organic-clay composites, on the contrary, things just go another way. No matter whether microfractures develop nearby or not, nanopores could always stably exist (Fig. 7e, f). It suggests that clay layers probably be obstacle to nanopores connecting outside, meaning that organic-clay composites could make pore connectivity worse. However, the mechanisms of the different types of composites decreasing pore connectivity are quite different. For example, band-like composites depend on clay layers to isolate the nanopores distributed in the two sides of clay layers (banded blank in Fig. 6 B_2 and Fig. 7 E_1). For another, most of deformed composites are in the shape of shrunk ends (Fig. 4b, g and Fig. 5h), which contribute to remain whole composites isolated. In addition, most deformations just bend the clay layers rather than crack them due to the plasticity of clay layers, thus ensuring the integrality of composites (Fig. 4b, g, Fig. 5h, and Fig. 7e, f). In addition, by reason of the specificity of the structure, "cardhouse" composites could keep the structure stable under geostress (Day-Stirrat et al. 2008). What is more, almost no microfractures developed neighboring this type of composites (Fig. 4c, i, and Fig. 5b). This is probably being driven by the various

Table 3 The pore parameter characteristics of statistical regions in Fig. 7

Location	Pore count	Average pore area (nm^2)	Average pore diameter (nm)
C_1	699	107	18
D_1	900	121	18
E_1	128	154	18
F_1	699	91	17

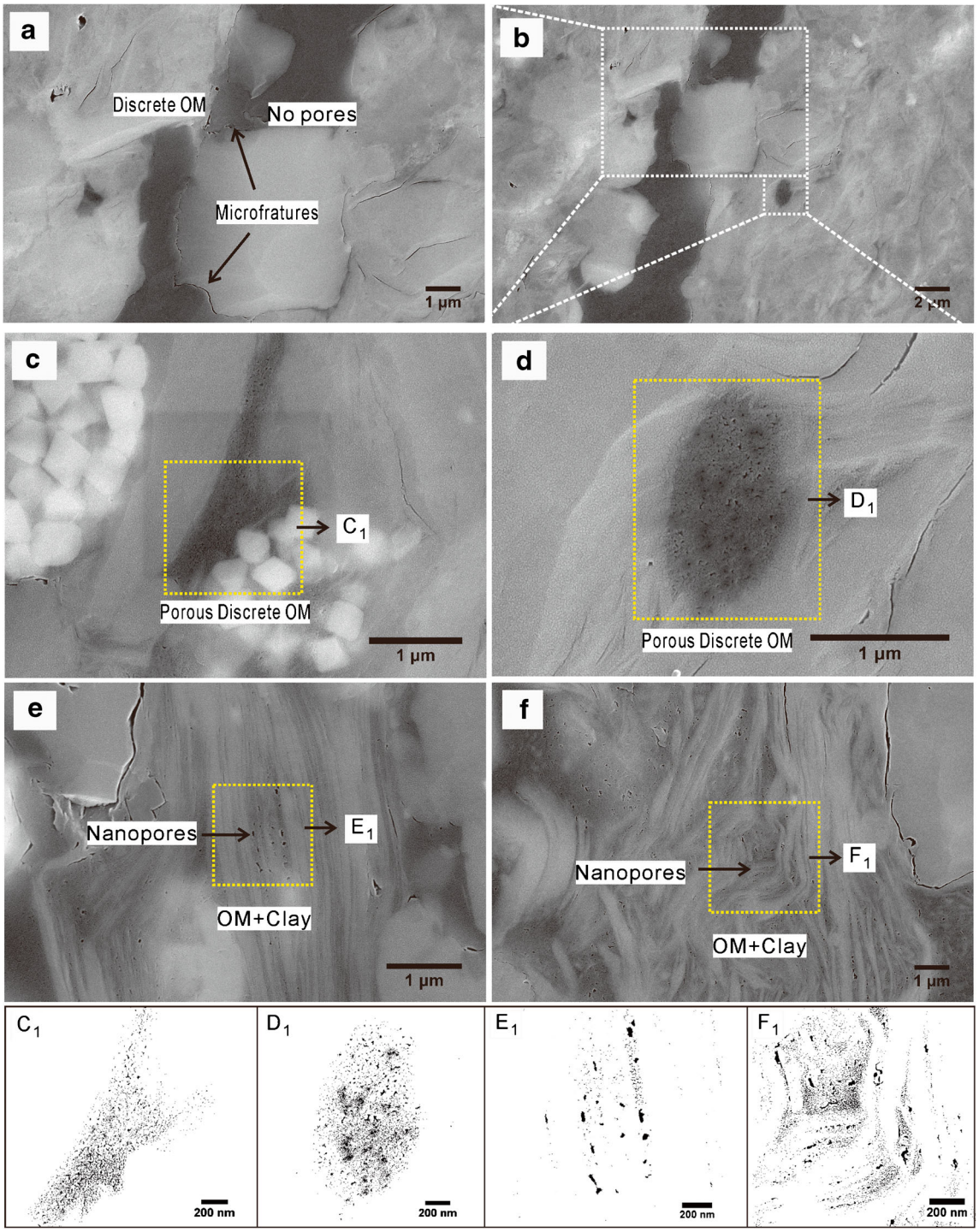

Fig. 7 The nanopores characteristics in discrete OM and organic-clay composites for C_1n shales. The four white dashed rectangles were the selected regions for the statistics of nanopores. C_1–D_1denoted the grayscale maps of corresponding regions

directions of clay layers in "cardhouse" composites, which contributes to disperse geostress to avoid stress concentrating on one direction and resulting in microfractures (Lagely 1989).

To sum up, although the nanopores in organic-clay composites are also generated by thermal evolution of OM, the evolution of nanopores in composites present different trends with the pores in discrete OM. The reason for the responsibility is the role of clay layers in composites during nanopores evolution. As illustrated by Fig. 8, compared to discrete OM, the clay layers restrict the development of nanopores in composites at first by suppressing the growth of nanopores (Fig. 8e compared to b). After emergence of nanopores in composites, the clay layers play a key role in disengaging the channel

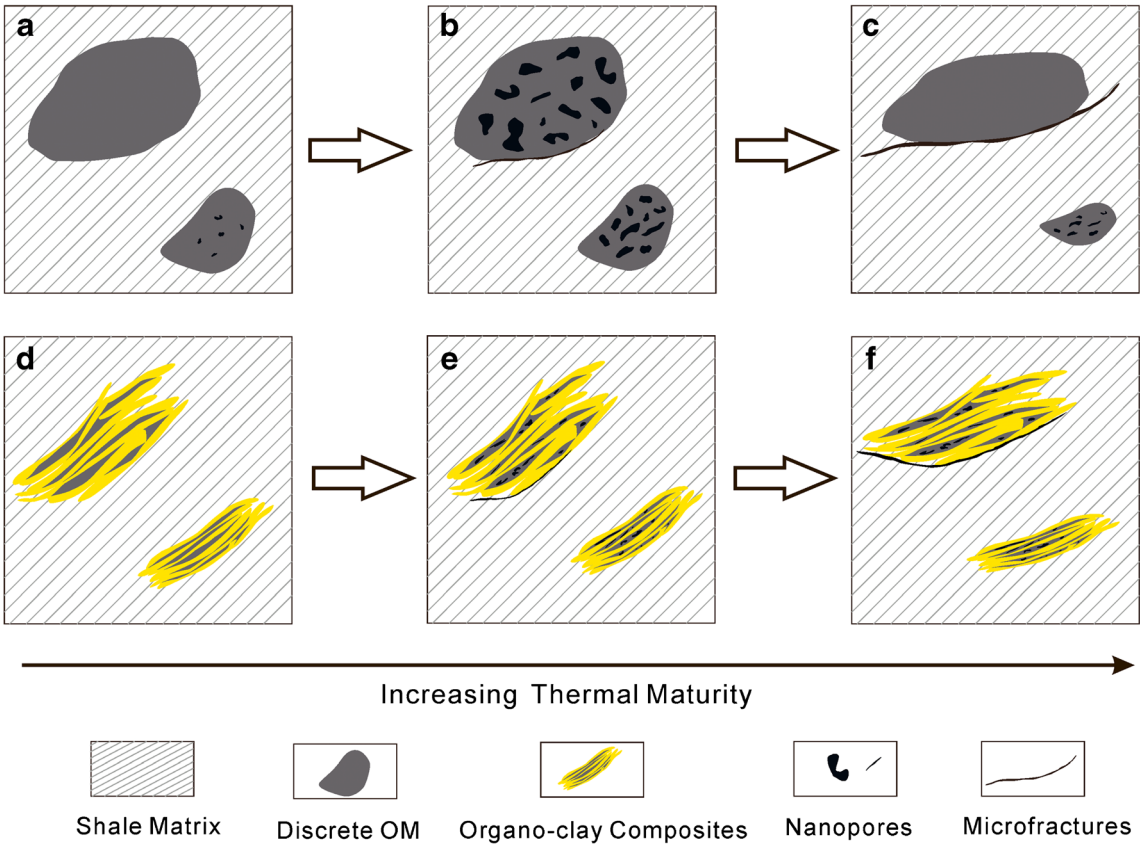

Fig. 8 The schematic diagram of nanopores evolution in discrete OM (**a**–**c**) and organic-clay composites (**d**–**f**)

access to the outside. The isolation of clay layers on nanopores in composites could maintain the internal pressure in pores, which prevent the pore space from compaction. In over-maturation stage, the composites protect the nanopores from collapse and compaction regardless of whether microstructures developed nearby underlying the strong adsorption of clay layers on organic carbon and the stable structure of inorganic-organic interaction to resist overburden pressure (Fig. 8f compared to c). Logically, an inference could be obtained that there still exist hydrocarbons in the nanopores located in organic-clay composites. Therefore, besides the pores in discrete OM, connecting the nanopores in composites is also critical for improving gas yield.

The manipulation of stress on nanopores distribution

The nanopores in discrete OM under stress

Most of discrete OM particles are observed being adjacent to brittle minerals (Fig. 9). Due to the weak resistance of organic matter to stress, the contact between organic matter and brittle minerals often causes deformation of organic matter to a certain extent (Schieber et al. 2010; Wang 2020). The additional stress from impinging mineral flattens OM-hosted pores in a direction perpendicular to the applied maximum stress (Fig. 9b, d, g, h), and the closer the OM-hosted pores are to the impinging mineral, the stronger the deformation (Wang

Table 4 The pore parameter characteristics of statistical regions in Fig. 10

Location	Pore counts	Pore area (nm^2)	Aspect ratio	Average pore diameter (nm)
A_1	28	240	1.81	21
A_2	92	296	1.78	21
A_3	93	432	1.64	23
B_1	19	168	1.98	20
B_2	27	280	1.94	25
B_3	46	536	1.86	32
B_4	58	918	1.85	42

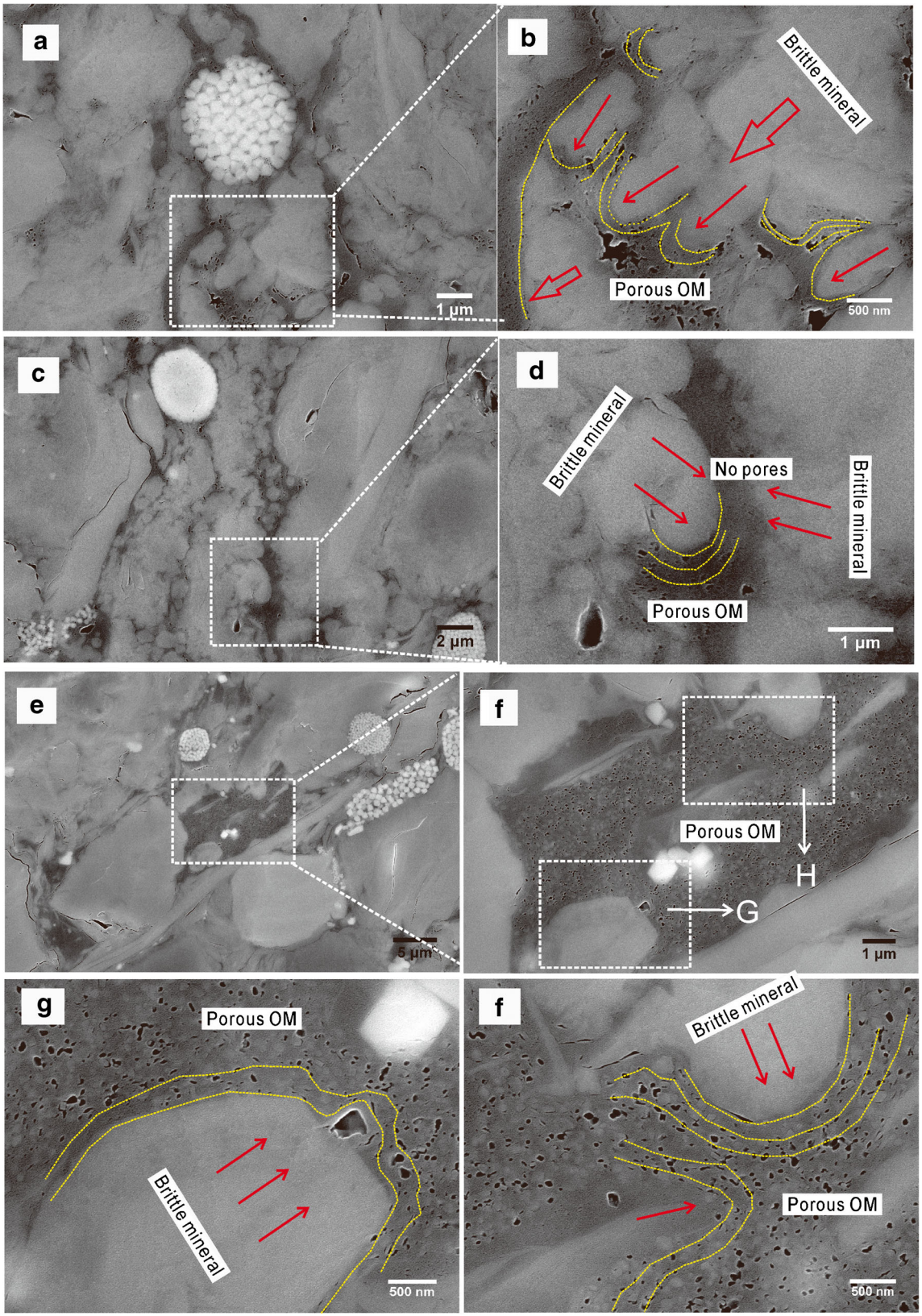

Fig. 9 The nanopores in discrete OM under compressive stress. The red arrows denoted the direction of additional stress, and the yellow dotted lines denoted the arrangement of nanopores

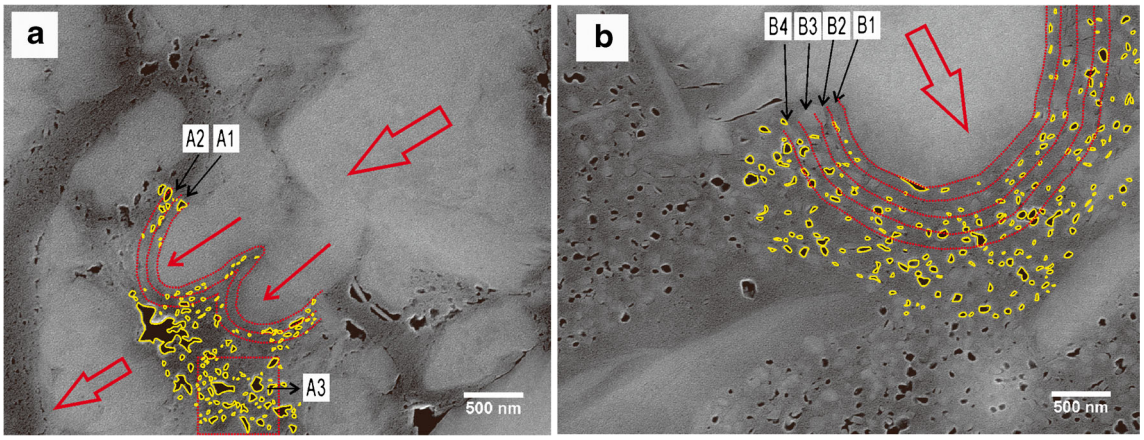

Fig. 10 The outlines of nanopores in discrete OM and the distribution characteristics. The red arrows denoted the direction of additional stress, and the yellow curves profile the outlines of the nanopores. The regions A_1, A_2, and B_1–B_4 are divided by the red curves paralleling to the boundary of the imposed mineral as a width of 100 nm. The region A_3 represents the pores in a tensile environment or stress-free state

2020). If the porous OM particles are compressed severely by the minerals of both sides, the pores tend to disappear (Fig. 9d). To certify the effects of deformation on the size and geometry of nanopores, the images of Fig. 9b and h are utilized to quantitatively evaluate the structural changes. As shown in Fig. 10 and Table 4, the nanopores distributed near the imposed minerals are profiled to analysis the pore parameters, including the pore counts, pore area, aspect ratio of fitted ellipses, and average pore diameter in the regions marked by red curves and box. The statistical results show that with far away from the pressure source (from A1 to A3 and B1 to B4), pore counts, pore area, and average pore diameter present obvious increasing trends, while the aspect ratio of fitted ellipses appears decreasing, indicating the manipulation of additional stress on diminishing the sizes of nanopores and orienting with their long axes tending to parallel the boundary of the imposed mineral. By comparison, when the OM particles are in tensile environment or in stress-free state, pores tend to be regular sphere (region A3). This is because the volume expending for reaction of hydrocarbon generation would be an isotropic process if no addition stress intervenes, which profits to form near-spherical pores. In addition, the distribution of nanopores under tensile stress or stress-free state (region A3) is more homogeneous than the pores under compressive stress (regions A1 and A2), reflecting the significant contribution of additional compressive stress to strengthening the heterogeneity of nanopore distribution.

Table 5 The pore parameter characteristics of statistical regions in Fig. 11

Location	Pore count	Average pore area (nm^2)	Average pore diameter (nm)
B_1	102	877	44
B_2	64	526	36
D_1	311	610	40
D_2	200	933	40

The nanopores in organic-clay composites under stress

As previously mentioned, compared with the nanopores in discrete OM, the nanopores in organic-clay composites perform different evolutionary trends because of the existence of clay layers. Similarly, under stress, original organic-clay composites also behave with different deformation trends (Zhu et al. 2020). As Fig. 11 and Fig. 12 present, the organic-clay composites would produce distortion between layers for stress action, and too large stress will lead to tearing the layers. Due to the layer structure of clay minerals (such as illite and smectite), most of the composites present different deformation under different stress states. Under compressive stress, which most come from brittle minerals, the OM between clay layers almost develop no pores (Fig. 12a), probably stem from pressure-retarding effect of hydrocarbon generation (Wu et al. 2016), while under tensile stress, quantities of spherical-ellipsoidal nanopores are observed in OM between clay layers (Fig. 11b, d, and Fig. 12b, d). Two reasons could produce the tensile environment: (a) the growth of mineral particles; (b) the deformation of composites. From the SEM images (Fig. 11 and Fig. 12), the pyrites in organic-clay composites are stuck between the clay layers, which induces the OM between layers are in a tensile environment. Significantly, the OM pores developed very well in the interspace between clay with supporting of pyrite particles (Fig. 11b, d, and Fig. 12d). More remarkably, the size of pyrites directly influences the pore size. As shown by Table 5, the average pore diameter of B_1 (44 nm) is larger than B_2 (36 nm), and the sizes of corresponding imposed pyrite are 1.46 μm and 0.75 μm (Fig. 11B), respectively, which sufficiently support that tensile environment contributes to pore growth. For D_1 and D_2, the average pore diameters are the same (40 nm) because of the similar pyrite size (1.25 μm and 1.21 μm) (Fig. 11d). The second reason responsible for the

Table 6 The pore parameter characteristics of statistical regions in Fig. 12

Location	Pore count	Average pore area (nm^2)	Average pore diameter (nm)
B_1	136	107	13
B_2	131	180	17
D_1	211	21	8
D_2	267	36	10

tensile environment originates from the deformation of composites. As Fig. 12b shown, partially deformed composites present lenticular shape, featured by shrinking ends and corpulent core. In general, the core of composites is in a tensile environment, while the ends are in the compressive environment, which decides that nanopores prefer to be developed in the core but not the ends (Fig. 12b). The average pore diameters of B_1 (13 nm) and B_2 (17 nm) (Table 6) also demonstrate that the core of composites is more beneficial to pore growth than the ends. In addition, partial composites could generate a tensional environment under shear stress (Fig. 12b (yellow dotted lines in the bottom) and D_2). Take Fig. 12d as an example. In the central region, no pores are observed, while for region D_2, the shear stress facilitates clay layers deformed as Z-shaped, further forming a tensile environment between layers and develop large amounts of nanopores

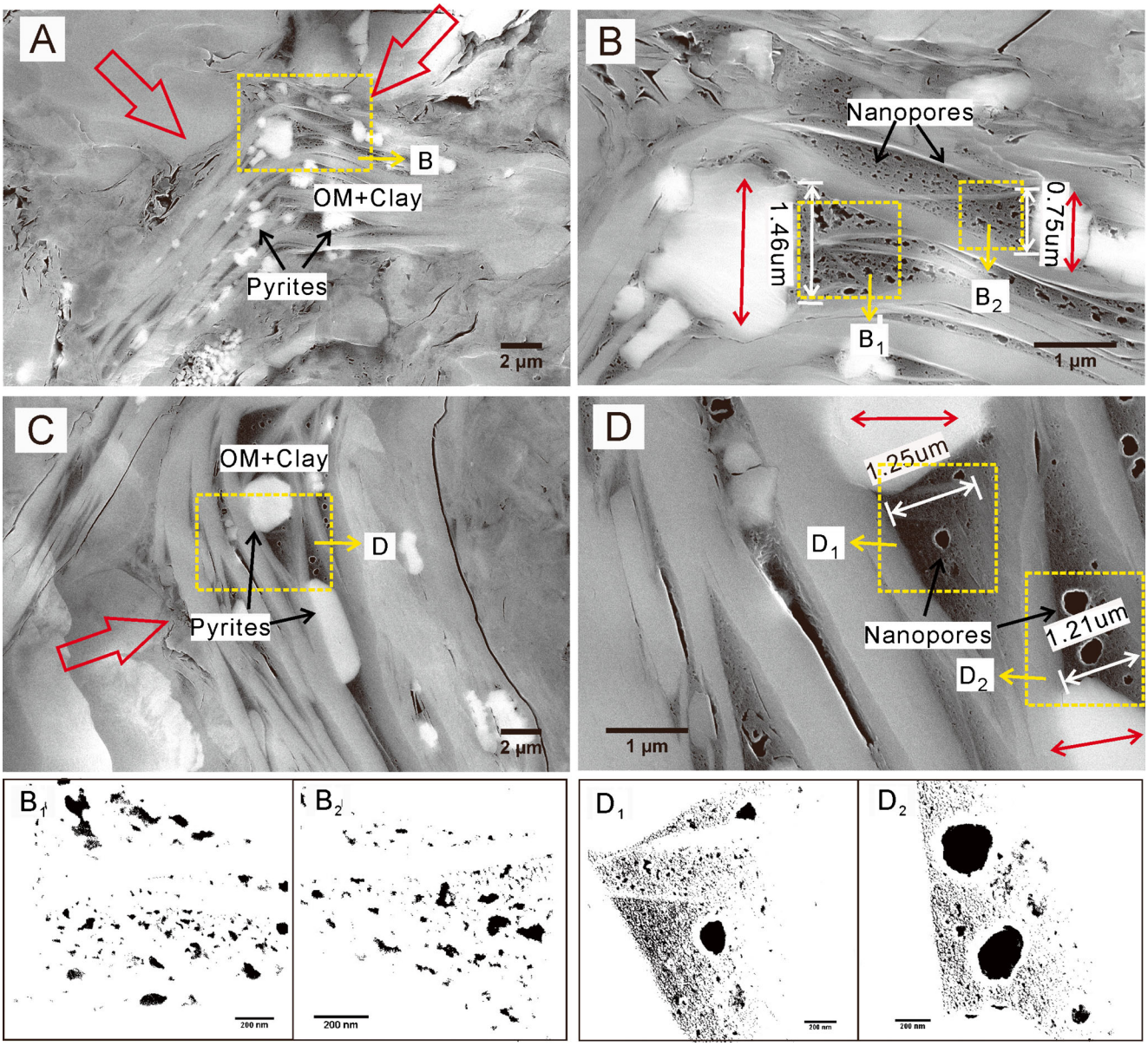

Fig. 11 The nanopores in organic-clay composites under additional stress for S_1l shales. The red arrows denoted the direction of additional stress, and the yellow dashed rectangles were the selected regions for the statistics of nanopores. B_1–D_2 denoted the grayscale maps of corresponding regions. The regions B_1–D_2 are in the tensile environment caused by the growth of pyrite particles

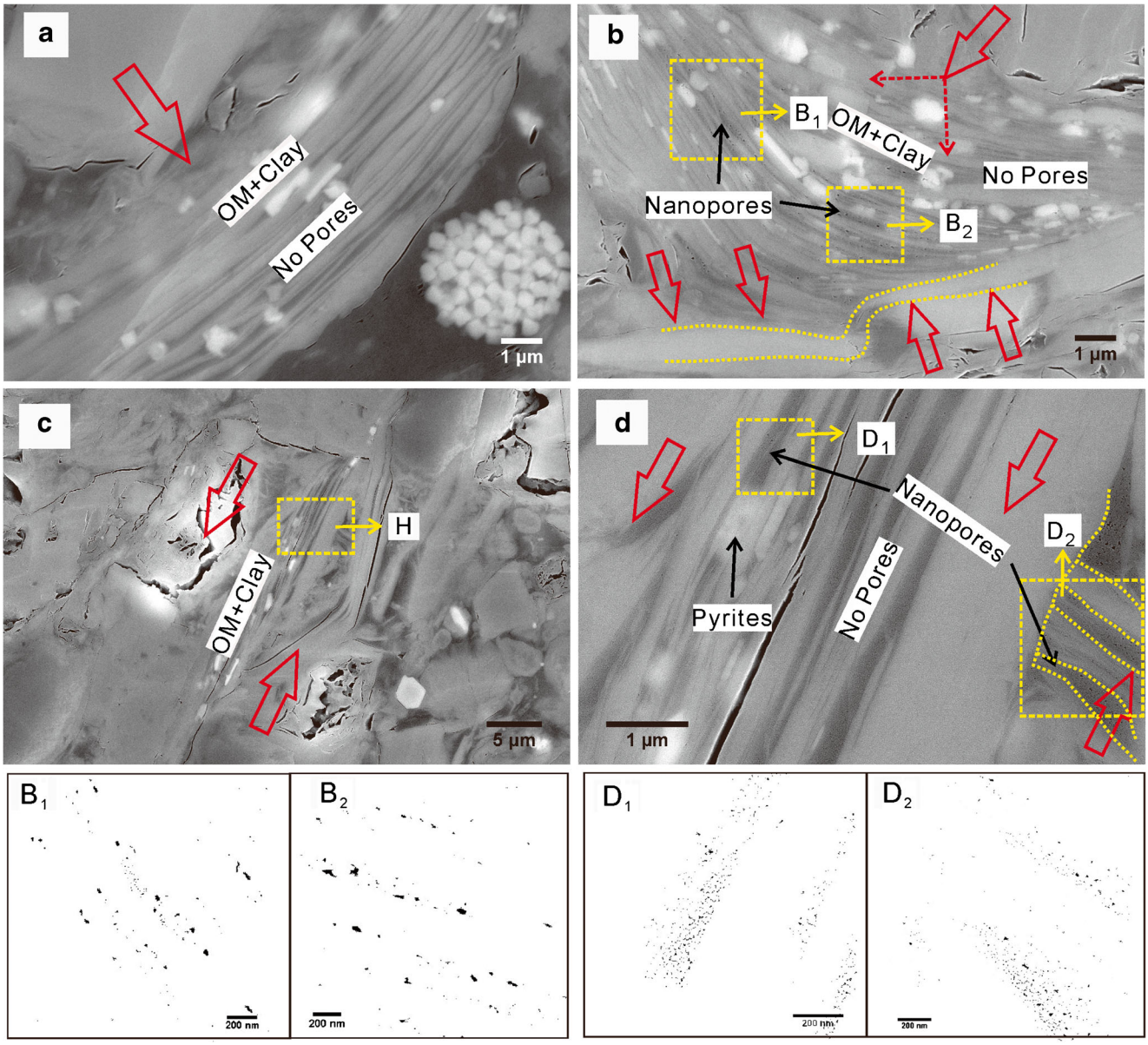

Fig. 12 The nanopores in organic-clay composites under additional stress for ϵ_1n shales. The red arrows denoted the direction of additional stress, and the yellow dashed rectangles were the selected regions for the statistics of nanopores. B_1–D_2 denoted the grayscale maps of corresponding regions. The regions B_1, B_2, and D_2 are in the tensile environment caused by the deformation of clay layers under shear stress, and the region D_1 is in the tensile environment caused by the growth of pyrite particles

(more than two hundred). In comparison, although nanopores are also developed in region D_1, the reason is different for the formation of the tensile environment (growth of pyrites).

Overall, under additional stress, both discrete OM and organic-clay composites appear deformation, contributing to the heterogeneity of nanopores. At the nano- and microscale, stress associated with the mineral framework introduces additional forces on OM particles and organic-clay composites, resulting in different deformation for the two objects. The nanopore features in discrete OM, including the pore size, geometry, and orientation, could be significantly modified by the imposition of compressive stress. Since the intervention of clay minerals, different responses to different additional stresses are reflected by the development characteristics of nanopores in organic-clay composites, including distribution and size. That suggests the additional stress is a significant factor for the development of nanopores either in discrete OM or organic-clay composites.

Conclusions

In this research, two formations of potential shales (S_1l and ϵ_1n) were selected to explore the evolution of nanopores in

discrete OM and organic-clay composites. The conclusions obtained from this study are as follows:

(1) The discrete OM mostly fills between skeleton particles and present irregular shapes. The organic-clay composites, exhibiting various morphologies, could be classified into two types: primary and deformed. The primary composites maintain the original forms at the sedimentation, mainly including band-like (face/face contacts) and "cardhouse" (edge/face contacts). However, most composites are deformed under additional stress and exhibit various morphological structures.
(2) The nanopores in discrete OM and organic-clay composites present different development characteristics with increasing maturity. During the growth of nanopores, the nanopores in composites are smaller than the pores in discrete OM, which results from the restriction of clay layers on nanopores developing. With further increasing maturity, nanopores in discrete OM tend to disappear because of more complete gas expulsion (pore collapse) under framework compaction, while the isolation of clay layers on nanopores in composites could protect the nanopores from collapse or compaction.
(3) The nanopores in discrete OM under compressive stress are oriented with their long axes tending to parallel the boundary of the imposed mineral. For organic-clay composites, the OM between clay layers almost develop no pores under compressive stress, while under tensile stress, quantities of spherical-ellipsoidal nanopores are observed, and pores are larger in more tensile environment. All above indicates the manipulation of additional stress on the development of nanopores in discrete OM and organic-clay composites.

Funding This work is supported by the National Natural Science Foundation of China (41802143) and the Doctoral Program of Henan University of Engineering (DKJ2018014).

Declarations

Conflict of interest The author(s) declare that they have no competing interests

References

Alcover JF, Qi Y, Al-Mukhtar M et al (2000) Hydromechanical effects: (I) on the Na-smectite microtexture. Clay Miner 35(3):525–536

Berthonneau J, Grauby O, Abuhaikal M, Pellenq RJM, Ulm FJ, van Damme H (2016) Evolution of organo-clay composites with respect to thermal maturity in type II organic-rich source rocks. Geochim Cosmochim Acta 195:68–83

Bu H, Yuan P, Liu H, Liu D, Liu J, He H, Zhou J, Song H, Li Z (2017) Effects of complexation between organic matter (OM) and clay mineral on OM pyrolysis. Geochim Cosmochim Acta 212:1–15

Cai J, Song M, Lu L et al (2013) Organo-clay complexes in source rocks—a natural material for hydrocarbon generation. Mar Geol Quat Geol 33(3):123–131

Chalmers GR, Bustin RM, Power IM (2012) Characterization of gas shale pore systems by porosimetry, pycnometry, surface area, and field emission scanning electron microscopy/transmission electron microscopy image analyses: Examples from the Barnett, Woodford, Haynesville, Marcellus, and Doig units. AAPG Bull 96(6):1099–1119

Chen J, Xiao XM (2014) Evolution of nanoporosity in organic-rich shales during thermal maturation. Fuel 129:173–181

Chen GJ, Yen MC, Wang JM, Lin JJ, Chiu HC (2008) Layered inorganic/enzyme nanohybrids with selectivity and structural stability upon interacting with biomolecules. Bioconjug Chem 19(1):138–144

Chen SB, Zuo ZX, Zhu YM et al (2015) Applicability of the testing method for the maturity of organic matter in shale gas reservoirs. Nat Gas Geosci 26(3):564–574

Curtis ME, Cardott BJ, Sondergeld CH, Rai CS (2012a) Development of organic porosity in the Woodford Shale with increasing thermal maturity. Int J Coal Geol 103:26–31

Curtis ME, Sondergeld CH, Ambrose RJ, Rai CS (2012b) Microstructural investigation of gas shales in two and three dimensions using nanometer-scale resolution imaging. AAPG Bull 96(4):665–677

Day-Stirrat RJ, Loucks RG, Milliken KL et al (2008) Phyllosilicate orientation demonstrates early timing of compactional stabilization in calcite-cemented concretions in the Barnett Shale (Late Mississippian), Fort Worth Basin, Texas (U.S.A). Sediment Geol 208(1-2):27–35

Devey R, Curtis CD (1989) Mossbauer and chemical investigations of mud rock. Clay Miner 24(1):53–65

Dong DZ, Wang YM, Li XJ et al (2016) Breakthrough and prospect of shale gas exploration and development in China. Nat Gas Ind 36(1):19–32

Gu Y, Wan Q, Qin Z, Luo T, Li S, Fu Y, Yu Z (2017) Nanoscale pore characteristics and influential factors of niutitang formation shale reservoir in Guizhou province. J Nanosci Nanotechnol 17(9):6178–6189

Gu Y, Wan Q, Yu W, Li X, Yu Z (2018) The effects of clay minerals and organic matter on nanoscale pores in Lower Paleozoic shale gas reservoirs, Guizhou, China. Acta Geochim 37(6):791–804

Guo H, Jia W, Peng Pa et al (2014) The composition and its impact on the methane sorption of lacustrine shales from the Upper Triassic Yanchang Formation, Ordos Basin, China. Mar Pet Geol 57:509–520

Guo C, Xu J, Wu K, Wei M, Liu S (2015) Study on gas flow through nano pores of shale gas reservoirs. Fuel 143:107–117

Hu Q, Ewing RP, Dultz S (2012) Low pore connectivity in natural rock. J Contam Hydrol 133:76–83

Jia W, Segal E, Kornemandel D, Lamhot Y, Narkis M, Siegmann A (2002) Polyaniline-DBSA/organophilic clay nanocomposites: synthesis and characterization. Synth Met 128(1):115–120

Kelemen SR, Fang HL (2001) Maturity trends in raman spectra from kerogen and coal. Energy Fuel 15(3):653–658

Kennedy MJ, Wagner T (2011) Clay mineral continental amplifier for marine carbon sequestration in a greenhouse ocean. Proc Natl Acad Sci U S A 108:9776–9781

Kennedy MJ, Pevear DR, Hill RJ (2002) Mineral surface control of organic carbon in black shale. Science 295:657–660

Kennedy MJ, Löhr SC, Fraser SA, Baruch ET (2014) Direct evidence for organic carbon preservation as clay-organic nanocomposites in a Devonian black shale; from deposition to diagenesis. Earth Planet Sci Lett 388:59–70

King HE, Eberle APR, Walters CC et al (2015) Pore architecture and connectivity in gas shale. Energy Fuel 29(3):1375–1390

Lagely G (1989) Principles of flow of kaolin and bentonite dispersions. Appl Clay Sci 4(2):105–123

Li J, Li X, Wu K, Wang X, Shi J, Yang L, Zhang H, Sun Z, Wang R, Feng D (2016) Water sorption and distribution characteristics in clay and shale: effect of surface force. Energy Fuel 30(11):8863–8874

Liu D, Xiao X, Tian H et al (2012) Sample maturation calculated using Raman spectroscopic parameters for solid organics: methodology and geological applications. Chin Sci Bull 58(11):1285–1298

Liu SG, Deng B, Zhong Y et al (2016) Unique geological features of burial and superimposition of the Lower Paleozoic shale gas across the Sichuan Basin and its periphery. Earth Sci Front 23(1):11–28

Liu AQ, Tang DJ, Shi XY et al (2019) Growth mechanisms and environmental implications of carbonate concretions from the ~ 1.4 Ga Xiamaling Formation, North China. J Palaeogeogr 8(3):285–300

Loucks RG, Reed RM, Ruppel SC, Jarvie DM (2009) Morphology, genesis, and distribution of nanometer-scale pores in siliceous mudstones of the Mississippian Barnett Shale. J Sediment Res 79(12): 848–861

Lu L, Cai J, Liu W et al (2013) Occurrence and thermostability of absorbed organic matter on clay minerals in mudstones and muddy sediments. Oil Gas Geol 34(1):16–26

Lu Y, Zhang J, Zhang P et al (2015) Gas accumulation conditions of Lower Cambrian Niutitang shale and prediction of potential zones in northwestern Guizhou. Mar Origin Pet Geol 20(2):37–44

Milliken KL, Rudnicki M, Awwiller DN, Zhang T (2013) Organic matter-hosted pore system, Marcellus Formation (Devonian), Pennsylvania. AAPG Bull 97(2):177–200

Nelson PH (2009) Pore-throat sizes in sandstones, tight sandstones, and shales. AAPG Bull 93(3):329–340

O'Brien NR (1971) Fabric of kaolinite and illite floccules. Clay Clay Miner 19(6):353–359

Rahman HM, Kennedy M, Löhr S, Dewhurst DN, Sherwood N, Yang S, Horsfield B (2018) The influence of shale depositional fabric on the kinetics of hydrocarbon generation through control of mineral surface contact area on clay catalysis. Geochim Cosmochim Acta 220: 429–448

Ruppert LF, Sakurovs R, Blach TP, He L, Melnichenko YB, Mildner DFR, Alcantar-Lopez L (2013) A USANS/SANS study of the accessibility of pores in the Barnett Shale to methane and water. Energy Fuel 27(2):772–779

Schieber J, Southard JB, Schimmelmann A (2010) Lenticular shale fabrics resulting from intermittent erosion of water-rich muds–interpreting the rock record in the light of recent flume experiments. J Sediment Res 80(1):119–128

Schoenherr J, Littke R, Urai JL, Kukla PA, Rawahi Z (2007) Polyphase thermal evolution in the Infra-Cambrian Ara Group (South Oman Salt Basin) as deduced by maturity of solid reservoir bitumen. Org Geochem 38(8):1293–1318

Sposito G, Skipper NT, Sutton R, Park SH, Soper AK, Greathouse JA (1999) Surface geochemistry of the clay minerals. Proc Natl Acad Sci U S A 96(7):3358–3364

Sun M, Yu B, Hu Q, Yang R, Zhang Y, Li B (2017) Pore connectivity and tracer migration of typical shales in south China. Fuel 203:32–46

Tang X, Zhang J, Jin Z, Xiong J, Lin L, Yu Y, Han S (2015) Experimental investigation of thermal maturation on shale reservoir properties from hydrous pyrolysis of Chang 7 shale, Ordos Basin. Mar Pet Geol 64:165–172

Theng BKG, Churchman GJ, Newman RH (1986) The occurence of interlayer clay-organic complexes in two New Zealand soils. Soil Sci 142(5):262–266

Tuschel D (2013) Raman spectroscopy of oil shale. Spectroscopy 28(3): 20–28

Wang G (2020) Deformation of organic matter and its effect on pores in mud rocks. AAPG Bull 103(1):21–36

Wang P, Jiang Z, Chen L, Yin L, Li Z, Zhang C, Tang X, Wang G (2016) Pore structure characterization for the Longmaxi and Niutitang shales in the Upper Yangtze Platform, South China: evidence from focused ion beam He ion microscopy, nano-computerized tomography and gas adsorption analysis. Mar Pet Geol 77:1323–1337

Wu Y, Ji L, He C, Zhang Z, Zhang M, Sun L, Su L, Xia Y (2016) The effects of pressure and hydrocarbon expulsion on hydrocarbon generation during hydrous pyrolysis of type-I kerogen in source rock. J Nat Gas Sci Eng 34:1215–1224

Zhu X, Cai J, Liu W, Lu X (2016) Occurrence of stable and mobile organic matter in the clay-sized fraction of shale: significance for petroleum geology and carbon cycle. Int J Coal Geol 160-161:1–10

Zhu X, Cai J, Wang G, Song M (2018) Role of organo-clay composites in hydrocarbon generation of shale. Int J Coal Geol 192:83–90

Zhu H, Ju Y, Huang C, Chen F, Chen B, Yu K (2020) Microcosmic gas adsorption mechanism on clay-organic nanocomposites in a marine shale. Energy 197:117256